

Article

# Analysis of a Series-Parallel Resonant Converter for DC Microgrid Applications

Bor-Ren Lin

Department of Electrical Engineering, National Yunlin University of Science and Technology, Yunlin 640, Taiwan; linbr@yuntech.edu.tw

**Abstract:** An input-series output-parallel soft switching resonant circuit with balance input voltage and primary-side current is studied and implemented for direct current (DC) microgrid system applications. Two resonant circuits are connected with input-series and output-parallel structure to have the advantages of low voltage stresses on active devices and low current stresses on power diodes. A balance capacitor is adopted on high voltage side to balance two input capacitor voltages. The *LLC* (inductor–inductor–capacitor) resonant circuit cells are employed in the converter to have soft switching operation for power semiconductors. The magnetic coupling component is adopted on the primary-side to automatically realize current balance of the two resonant circuits. In the end, a laboratory hardware circuit is built and tested. Experiments demonstrate and prove the validity of the resonant converter.

**Keywords:** series-parallel resonant converter; zero-voltage switching; DC microgrid



**Citation:** Lin, B.-R. Analysis of a Series-Parallel Resonant Converter for DC Microgrid Applications. *Processes* **2021**, *9*, 542. <https://doi.org/10.3390/pr9030542>

Academic Editor: Chang-Hua Lin

Received: 22 February 2021

Accepted: 17 March 2021

Published: 18 March 2021

**Publisher's Note:** MDPI stays neutral with regard to jurisdictional claims in published maps and institutional affiliations.



**Copyright:** © 2021 by the author. Licensee MDPI, Basel, Switzerland. This article is an open access article distributed under the terms and conditions of the Creative Commons Attribution (CC BY) license (<https://creativecommons.org/licenses/by/4.0/>).

## 1. Introduction

High efficiency power converters were widely presented and discussed for modern industry products [1,2]. For high power demand, power converters with high input voltage have been proposed for DC microgrid systems and DC light rail transportation power units. The input voltage may be higher than 750 or 1500 V. The control strategies and basic circuit topologies in DC microgrid have been presented and discussed in detail in [3,4]. Power semiconductors with high voltage rating capability have high cost, low frequency operation and large conduction losses. Therefore, the circuit size cannot be reduced due to limited switching frequency. To overcome this problem, the circuit topologies with series-connected switches or converters [5–12] and multilevel converters [13–20] can adopt low voltage stress and high switching frequency operation power switches in high voltage input cases. Therefore, the voltage stress on active devices can be reduced in these circuit topologies. However, power switches may have an unbalanced voltage rating on these circuit topologies. Multilevel diode-clamped or flying circuit topologies have been developed for converters or inverters with balance voltage rating on power switches. The control scheme is usually based on duty cycle control [21,22] or variable frequency control [23,24] to regulate load voltage and implement soft switching operation on power devices. *LLC* (inductor–inductor–capacitor) resonant converters [25,26] have the benefits of high circuit efficiency and less switching loss. However, the main drawback of the parallel-connected resonant circuit is unbalanced resonant currents. Thus, the current stresses on input power switches and output diodes are different.

A series-parallel resonant converter is presented and accomplished to achieve the advantages of the balanced input capacitor voltages and balance diode currents on two resonant circuits. The resonant converter presented has two *LLC* circuits with series-parallel connection. To balance input voltages, a flying capacitor is employed on high voltage side. A current balance component based on a magnetic-coupling core is used between two resonant circuits to achieve current sharing on power diodes. Therefore, the voltage and current balance issues on power semiconductors are all accomplished

and achieved by using the voltage balance capacitor and magnetic-coupling component. Two resonant circuits are operated at inductive load. Thus, the soft switching operation on power semiconductors can be realized over the whole load range. Compared to past three-level circuit topologies in [13,19,21], this circuit topology has simpler control and less circuit components for high voltage input applications. Experiments of a laboratory circuit with 750~800 V input voltage, 24 V output voltage and 40 A load current are demonstrated to confirm the benefits of the circuit.

## 2. Presented Resonant Converter

Figure 1 gives the basic circuit diagram in a simplify DC microgrid. The input sources of the DC microgrid may be DC or AC utility systems and clean energy power systems such as solar power or wind power. The outputs of the DC microgrid may be the low or high power DC loads, AC motor drives, battery storage systems or light rail transit applications. For DC transportation or DC light rail transit system applications, the input DC bus voltage may be 750 or 1500 V. For local industry factory and residential house applications, the input DC bus voltage is 380 V. Thus, the DC bus voltage in the DC microgrid system may be 380, 750 and 1500 V for universal power demands. Therefore, the high voltage input DC–DC converters are needed for DC transportation or high power DC loads applications. The proposed converter is presented to meet the demand of these applications.

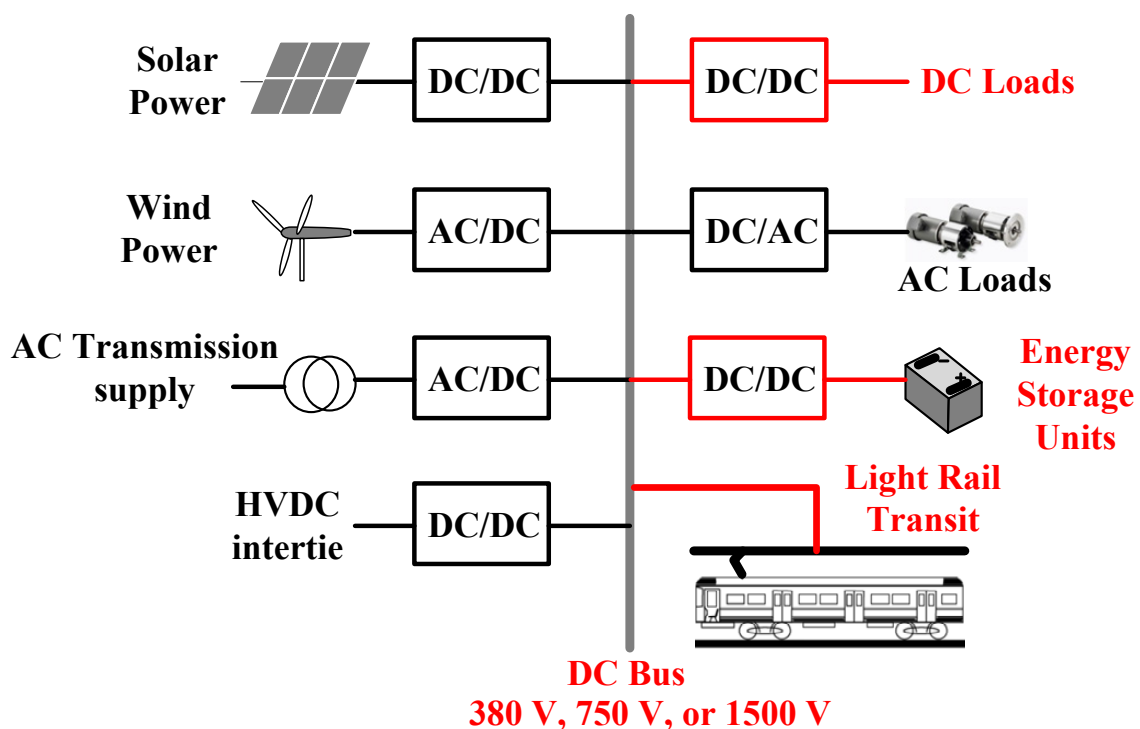
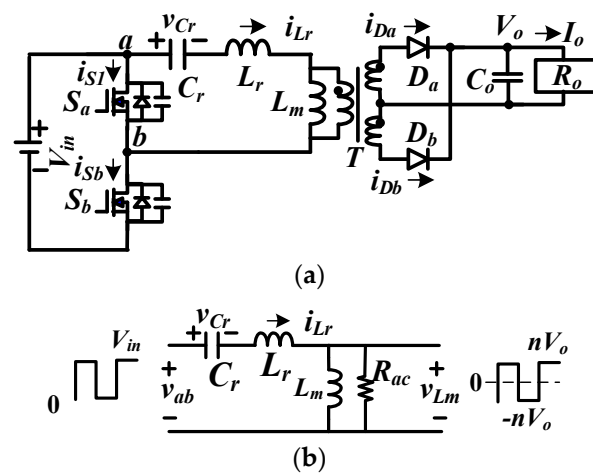


Figure 1. Simplified circuit schematic of a DC microgrid system.

### 2.1. Circuit Characteristics of a Conventional Resonant Converter

Figure 2a provides the circuit structure of conventional LLC converter.  $L_m$ ,  $L_r$  and  $C_r$  are the magnetizing inductance, series resonant inductance and series resonant capacitance, respectively.  $D_a$  and  $D_b$  are rectifier diodes and  $S_a$  and  $S_b$  are power switches. Frequency modulation with constant duty cycle is employed to regulate load voltage  $V_o$  and produce the gate signals for  $S_a$  and  $S_b$ . The basic circuit analysis of LLC converter can be analyzed using the fundamental harmonic approach in [27]. When a LLC converter is operated at series resonant frequency, the resonant converter likes a high frequency isolated DC transformer with zero-voltage switching (ZVS) turn-on operation on power switches and zero-current switching (ZCS) turn-off operation on rectifier diodes. Fundamental

frequency harmonic approach is usually used to approximately derive voltage gain of the resonant circuit. The turn-on time of  $S_a$  and  $S_b$  equals half of the switching period so that a square signal with 0 and  $V_{in}$  voltage values are observed on  $v_{ab}$ . The root-mean-square fundamental voltage of  $v_{ab}$  can be calculated as  $\sqrt{2}V_{in}/\pi$ . However, the secondary winding current is a quasi-sinusoidal current so that  $v_{Lm}$  is a quasi-square voltage signal with  $nV_o$  and  $-nV_o$  voltage values. The root-mean-square value of  $v_{Lm}$  is derived as  $2\sqrt{2}nV_o/\pi$ . Figure 2b gives the ac equivalent circuit on the primary side. For high voltage applications, the Insulated Gate Bipolar Transistor (IGBT) devices with 1200 V voltage rating can be used for  $S_a$  and  $S_b$ , shown in Figure 2a. The switching frequency of IGBT devices, however, is normally less than 400 kHz, and IGBT devices have serious switching losses at turn-off instant.



**Figure 2.** Conventional resonant converter (a) circuit structure and (b) AC equivalent circuit on primary side.

## 2.2. Proposed LLC Resonant Converter

Figure 3 provides the circuit schematic of the LLC converter presented. The input voltage is about 750~800 V from DC microgrid or DC light rail power system. The converter developed has two LLC circuits with series–parallel structure. Thus, the voltage stress of  $S_a \sim S_d$  is reduced to  $V_{in}/2$  and the average current of  $D_a \sim D_d$  is reduced to  $I_o/4$ . The first LLC circuit have components  $S_a, S_b, C_{r,a}, L_{r,a}, T_a, D_a$  and  $D_b$ . The circuit components of the second LLC circuit are  $S_c, S_d, C_{r,b}, L_{r,b}, T_b, D_c$  and  $D_d$ .  $D_a \sim D_d$  are rectifier diodes.  $C_{r1}$  and  $C_{r2}$  are the resonant capacitances,  $L_{r,a}$  and  $L_{r,b}$  are resonant inductors and  $L_{m,a}$  and  $L_{m,b}$  are the magnetizing inductors.  $C_o, C_{in,a}$  and  $C_{in,b}$  are output capacitor and input split capacitors. Capacitor  $C_f$  is connected between points  $b$  and  $c$ . If  $S_a$  and  $S_c$  are in the on-state and  $S_b$  and  $S_d$  are in the off-state, then  $V_{Cf} = V_{Cin,a}$ . If  $S_a$  and  $S_c$  are turned off and  $S_b$  and  $S_d$  are turned on, then  $V_{Cf} = V_{Cin,b}$ . Since the turn-on times of  $S_a \sim S_d$  are identical and equal  $T_s/2$ , the average capacitor voltages are derived as  $V_{Cf} = V_{Cin,a} = V_{Cin,b} = V_{in}/2$ . Therefore, input split DC voltages  $V_{Cin,a}$  and  $V_{Cin,b}$  are well balanced in each switching cycle. For achieving current balance of two LLC circuits, a magnetic-coupling (MC) component [28] is employed to achieve current sharing. If the inductor currents are well balanced ( $|i_{Lr,a}| = |i_{Lr,b}|$ ), then the induced voltages  $V_{La} = V_{Lb} = 0$ . If the inductor currents are unbalanced (such as  $|i_{Lr,a}| > |i_{Lr,b}|$ ), then  $V_{La}$  is decreased to reduce  $i_{Lr,a}$  and  $V_{Lb}$  is increased to increase  $i_{Lr,b}$ . After  $|i_{Lr,a}| = |i_{Lr,b}|$ , the voltages  $V_{La}$  and  $V_{Lb}$  are reduced to zero. Thus,  $i_{Lr,a}$  and  $i_{Lr,b}$  can be automatically balanced under steady state by using the MC component. The switching frequency is regulated to adjust voltage gain of the LLC presented. Therefore,  $V_o$  is regulated at the reference voltage value  $V_{o,ref}$ .

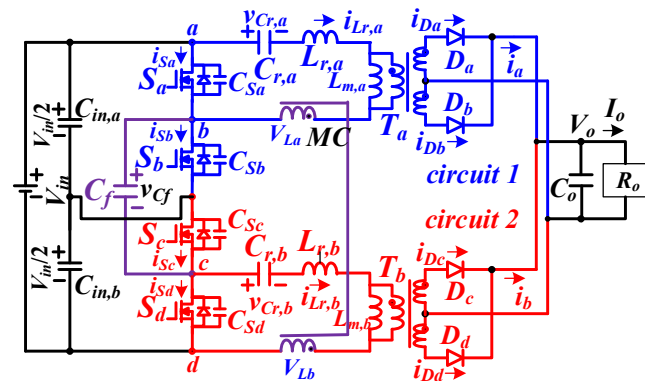


Figure 3. Circuit schematic of the inductor-inductor-capacitor (LLC) converter with series-parallel structure.

### 3. Principle of Operation

The circuit operations of the LLC converter presented are discussed from the following statements:

- (1) Transformers  $T_a$  and  $T_b$  have identical turn-ratio  $n_a = n_b = n_p/n_s$ ;
- (2) Inductances  $L_{m,a} = L_{m,b} = L_m$  and  $L_{r,a} = L_{r,b} = L_r$ ;
- (3)  $S_a \sim S_c$  have identical output capacitances  $C_{S_a} = C_{S_b} = C_{S_c} = C_{S_d} = C_S$ ;
- (4) Capacitances  $C_{in,a} = C_{in,b}$  and  $C_{r,a} = C_{r,b} = C_r$ .

The gate singles of power switches and key current and voltage waveforms per every switching cycle are given in Figure 4. From the conducting states of power devices, it can be observed that the converter presented has six operating steps for every switching cycle. Figure 5 gives the topological circuits for the six operating steps.

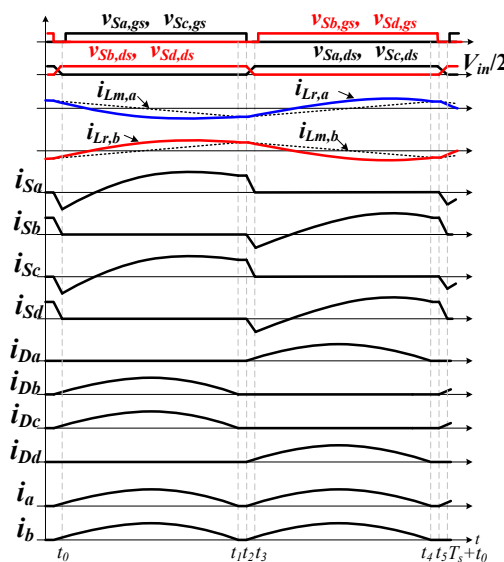


Figure 4. Main current and voltage signals of the LLC converter.

**Step 1 ( $t_0 \sim t_1$ ):** At time  $t < t_0$ ,  $S_a \sim S_d$  are all off and  $i_{Lr,a} > 0$  and  $i_{Lr,b} < 0$ . Thus,  $i_{Lr,a}$  discharges  $C_{S_a}$  and charges  $C_{S_b}$  and  $i_{Lr,b}$  discharges  $C_{S_c}$  and charges  $C_{S_d}$ . Due to  $i_{Lr,a} < i_{Lm,a}$  and  $i_{Lr,b} > i_{Lm,b}$ , the diode currents  $i_{D_b}$  and  $i_{D_c}$  are positive. After time  $t > t_0$ ,  $v_{C_{S_a}}$  and  $v_{C_{S_c}}$  decrease to zero voltage. Due to  $i_{S_a}(t_0) < 0$  and  $i_{S_c}(t_0) < 0$ , the body diodes of Metal-Oxide-Semiconductor Field-Effect Transistor (MOSFET)  $S_a$  and  $S_c$  conduct and  $v_{S_a,ds}$  and  $v_{S_c,ds}$  are zero voltage. Therefore, switches  $S_a$  and  $S_c$  can turn on to realize a soft switching characteristic. In step 1,  $i_{Lr,a} < i_{Lm,a}$  and  $i_{Lr,b} > i_{Lm,b}$ , the rectifier diodes  $D_c$  and  $D_d$  conduct, and  $V_{C_f} = V_{C_{in,a}}$ . Since the magnetizing voltages  $v_{Lm,a} = -nV_o$  and  $v_{Lm,b} = nV_o$ , the magnetizing currents  $i_{Lm,a}$  and  $i_{Lm,b}$  decrease and

increase, respectively. Under steady state operation and  $|i_{Lr,a}| = |i_{Lr,b}|$  operation, the induced voltages  $V_{La}$  and  $V_{Lb}$  across the MC cell are equal to zero.  $(L_{r,a}$  and  $C_{r,a})$  and  $(L_{r,b}$  and  $C_{r,a})$  are naturally resonant in converters 1 and 2, respectively with frequency  $f_r = 1/2\pi\sqrt{L_r C_r}$ . If  $f_s > f_r$ , then  $i_{Db}$  and  $i_{Dc}$  will decrease to zero before  $S_a$  and  $S_d$  turn off. After the step 1, circuit operation goes to step 2 when  $i_{Db} = i_{Dc} = 0$ . If  $f_s < f_r$ , then  $i_{Db}$  and  $i_{Dc}$  are still positive when  $S_a$  and  $S_c$  turn off. Under this condition, the circuit will go to step 3.

**Step 2 ( $t_1 \sim t_2$ ):** If  $f_s > f_r$ , then  $i_{Lr,a} = i_{Lm,a}$  and  $i_{Lr,b} = i_{Lm,b}$  at time  $t_1$ . Diodes  $D_a \sim D_d$  are turned off without reverse recovery current.  $(C_{r,a}, L_{r,a}$  and  $L_{m,a})$  and  $(C_{r,b}, L_{r,b}$  and  $L_{m,b})$  are resonant in circuits 1 and 2, respectively with frequency  $f_p = 1/2\pi\sqrt{(L_m + L_r)C_r}$ .

**Step 3 ( $t_2 \sim t_3$ ):** At  $t_2$ , power devices  $S_a$  and  $S_c$  turn off. Due to  $i_{Lr,a}(t_2) < 0$  and  $i_{Lr,b}(t_2) > 0$ ,  $C_{Sa}$  ( $C_{Sb}$ ) and  $C_{Sc}$  ( $C_{Sd}$ ) are charged (discharged) in step 3. Diodes  $D_a$  and  $D_d$  are forward biased to conduct load current. If the energies on  $L_{r,a}$  and  $L_{r,b}$  are greater than the energies on  $C_{Sa} \sim C_{Sd}$ , then  $v_{Sb,ds}$  and  $v_{Sd,ds}$  will decrease to zero at  $t_3$ .

**Step 4 ( $t_3 \sim t_4$ ):** At time  $t_3$ ,  $C_{Sb}$  and  $C_{Sd}$  discharge to zero voltage. Due to  $i_{Lr,a}(t_3) < 0$  and  $i_{Lr,b}(t_3) > 0$ , the body diodes of  $S_b$  and  $S_d$  conduct and Thus,  $S_b$  and  $S_d$  can turn on to realize ZVS operation. Diodes  $D_a$  and  $D_d$  conduct,  $v_{Lm,a} = nV_o$ ,  $v_{Lm,b} = -nV_o$ ,  $i_{Lm,a}$  increases, and  $i_{Lm,b}$  decreases.  $(L_{r,a}$  and  $C_{r,a})$  and  $(L_{r,b}$  and  $C_{r,b})$  are naturally resonant in each LLC circuit.

**Step 5 ( $t_4 \sim t_5$ ):** At time  $t_4$ , the magnetizing currents  $i_{Lm,a}$  and  $i_{Lm,b}$  equal  $i_{Lr,a}$  and  $i_{Lr,b}$ , respectively. Thus, the secondary-side diodes  $D_a \sim D_d$  are turned off without reverse recovery current loss.  $(L_{r,a}, C_{r,a}$  and  $L_{m,a})$  and  $(L_{r,b}, C_{r,b}$  and  $L_{m,b})$  are naturally resonant in each circuit, respectively.

**Step 6 ( $t_5 \sim T_s + t_0$ ):** At time  $t_5$ , power devices  $S_b$  and  $S_d$  turn off. Due to  $i_{Lr,a}(t_5) > 0$  and  $i_{Lr,b}(t_5) < 0$ ,  $C_{Sa}$  ( $C_{Sb}$ ) and  $C_{Sc}$  ( $C_{Sd}$ ) are discharged (charged) in step 6. The diodes  $D_b$  and  $D_c$  are conducting. If the energies on  $L_{r,a}$  and  $L_{r,b}$  is greater than the energies on  $C_{Sa} \sim C_{Sd}$ , then  $v_{Sa,ds}$  and  $v_{Sc,ds}$  will be decreased to zero at  $T_s + t_0$ .

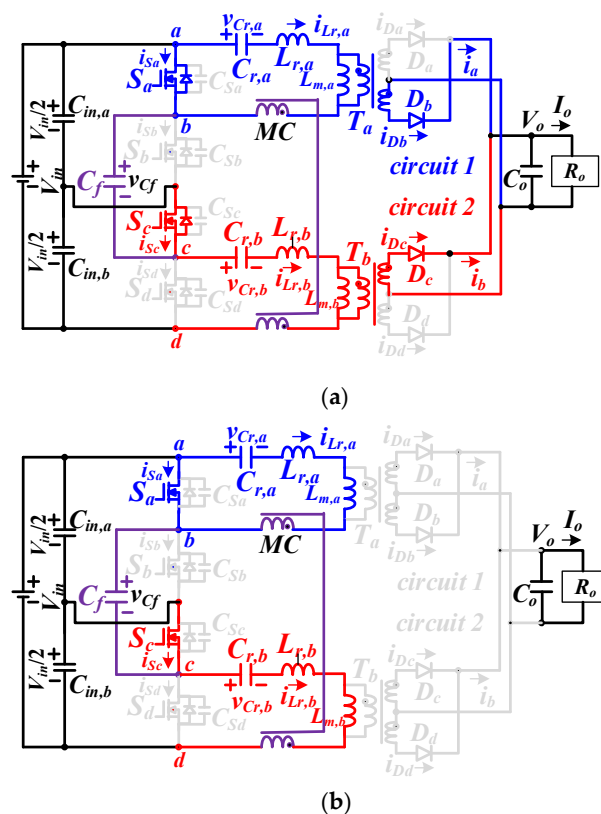
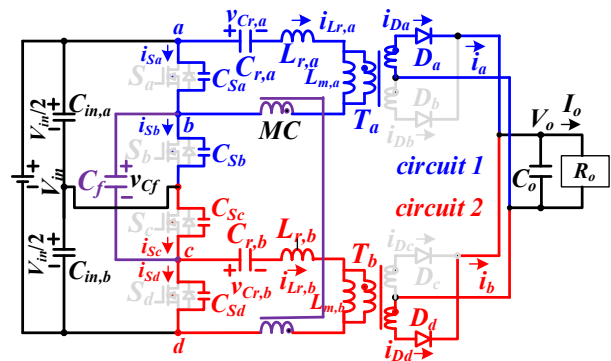
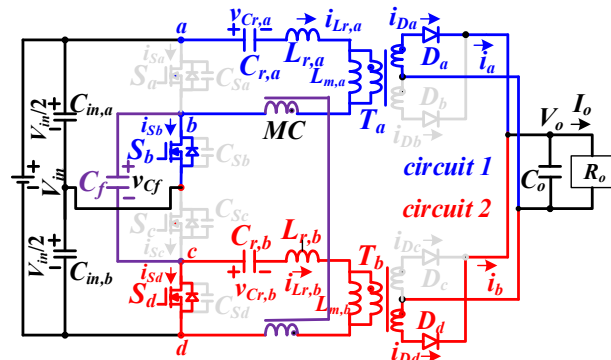


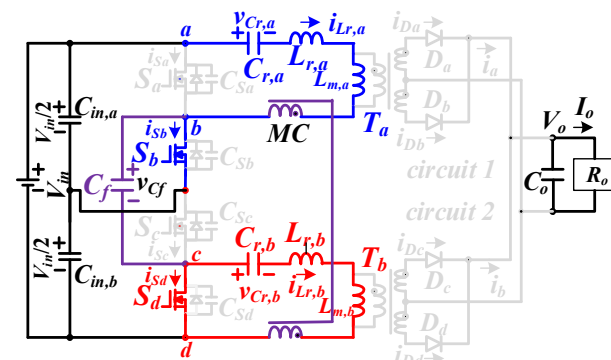
Figure 5. Cont.



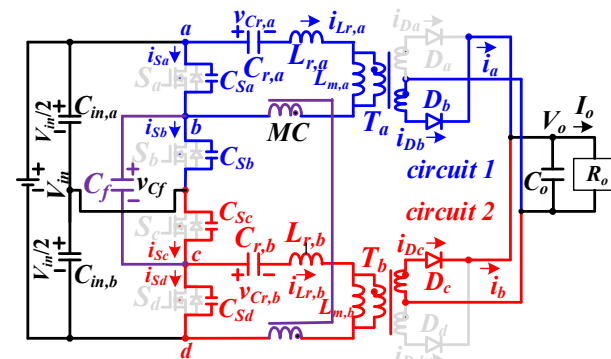
(c)



(d)



(e)



(f)

Figure 5. Equivalent circuits for each step (a) step 1, (b) step 2, (c) mode 3, (d) step 4, (e) step 5, (f) step 6.

#### 4. System Analysis and Design Example

Two LLC resonant circuits with series–parallel structure are adopted to decrease voltage stresses on power switches and current stresses on power diodes. A flying capacitor is employed to realize voltage balance on input capacitors. A magnetic-coupling component is connected between two LLC circuits to accomplish current sharing. In current balance condition and steady state operation, the primary and secondary voltages of the magnetic-coupling component equal zero. The magnetic-coupling component is ignored in the following discussion. Fundamental frequency analysis [27] is employed to obtain voltage gain of the converter presented. It is observed that  $v_{ab}$  and  $v_{cd}$  are square voltage waveforms. ( $L_{r,a}$  and  $C_{r,a}$ ) and ( $L_{r,b}$  and  $C_{r,b}$ ) are resonant on circuits 1 and 2 to generate two quasi-sinusoidal on  $i_{Lr,a}$  and  $i_{Lr,b}$ . The voltages  $v_{ab}$  and  $v_{cd}$  at the fundamental frequency are  $v_{ab,f} = v_{cd,f} = V_{in} \sin(2\pi f_s t) / \pi$ . If the circuit is operated at series resonant frequency, then the conducting time of  $D_a \sim D_d$  is equal to  $T_s/2$ . The secondary winding currents at fundamental frequency are derived as  $i_{Ta,sec} = i_{Tb,sec} = \pi I_o \sin(2\pi f_s t - \theta) / 4$ . The fundamental magnetizing voltages are given as  $v_{Lm,a,f} = v_{Lm,b,f} = 4nV_o \sin(2\pi f_s t - \theta) / \pi$ . The ac equivalent resistances  $R_{ac,a}$  and  $R_{ac,b}$  on primary-side of  $T_a$  and  $T_b$  are derived  $R_{ac,a} = R_{ac,b} = \frac{v_{Lm,a,f}}{i_{Ta,sec}/n} = 16(\frac{n}{\pi})^2 R_o$  ( $C_{r,a}$ ,  $L_{r,a}$ ,  $L_{m,a}$  and  $R_{ac,a}$ ) and ( $C_{r,b}$ ,  $L_{r,b}$ ,  $L_{m,b}$  and  $R_{ac,b}$ ) are resonant on each corresponding resonant tank. Figure 6a gives the resonant tank on the primary-side of resonant circuit 1. The ac voltage gain of the circuit developed can be expressed as.

$$|G(f_s)| = v_{Lm,a,f} / v_{ab,f} = 1 / \sqrt{[1 + \frac{1}{K_L}(1 - \frac{1}{F^2})]^2 + [Q(F - \frac{1}{F})]^2} \quad (1)$$

where  $f_r = 1/2\pi\sqrt{L_r C_r}$ ,  $K_L = L_{m,a}/L_{r,a}$ ,  $Q = \sqrt{L_r/C_r}/R_{ac,a}$  and  $F = f_s/f_r$ . From Equation (1), the gain voltage between the different load ( $Q$ ) and normalized switching frequency ( $F$ ) under  $K_L = 8$  is provided in Figure 6b.

The converter studied is proved by a prototype based on the following conditions: 750 V~800 V input voltage, 24 V output voltage, 40 A load current and 120 kHz series resonant frequency by  $C_{r,a}$  and  $L_{r,a}$ .  $T_a$  and  $T_b$  are implemented by magnetic cores TDK EER-42 with 24 primary winding turns and 3 secondary winding turns. Based on the turn-ratio of  $T_a$  and  $T_b$ , the maximum and minimum voltage gains of LLC converter are provided in (2).

$$G_{dc,max} = \frac{4n(V_o + V_f)}{V_{in,min}} \approx 1.06, \quad G_{dc,min} = \frac{4n(V_o + V_f)}{V_{in,max}} \approx 1 \quad (2)$$

where  $V_f = 0.8$  V on  $D_a \sim D_d$ . At 100% output power,  $R_{ac,a}$  and  $R_{ac,b}$  are derived in (3).

$$R_{ac,a} = R_{ac,b} = 16(\frac{n}{\pi})^2 R_o \approx 62.25\Omega \quad (3)$$

In the prototype, the selected  $Q$  is 0.3 to obtain the maximum gain at low voltage input under full load. The inductor ratio  $K_L$  is selected as 8 to reduce the circulating current losses on magnetizing inductor. With the given  $K_L$ ,  $f_r$  and  $Q$ , the components  $L_{r,a}$ ,  $L_{r,b}$ ,  $C_{r,a}$ ,  $C_{r,b}$ ,  $L_{m,a}$  and  $L_{m,b}$  are derived:

$$L_{r,a} = L_{r,b} = \frac{QR_{ac,a}}{2\pi f_r} \approx 25\mu H \quad (4)$$

$$C_{r,a} = C_{r,b} = \frac{1}{4\pi^2 L_{r1} f_r^2} \approx 70nF \quad (5)$$

$$L_{m,a} = L_{m,b} = K_L L_{r,a} \approx 200\mu H \quad (6)$$

The root-mean-square magnetizing currents  $i_{Lm,a,rms}$  and  $i_{Lm,b,rms}$  at series resonant frequency 120 kHz are calculated as

$$i_{Lm,a,rms} = i_{Lm,b,rms} = \frac{1}{2\sqrt{3}} \frac{nV_o}{2f_s L_{m,a}} \approx 1.155A \quad (7)$$

The primary-side root-mean-square load currents at full load are expressed as

$$i_{Ta,pri,rms} = i_{Tb,pri,rms} = \frac{\pi}{4\sqrt{2}} \frac{I_o}{n} \approx 2.78A \quad (8)$$

Therefore, the root-mean-square resonant inductor currents are obtained as

$$i_{Lr,a,rms} = i_{Lr,b,rms} = \sqrt{i_{Lm,a,rms}^2 + i_{Ta,pri,rms}^2} \approx 3A \quad (9)$$

Due the circuit structure, the voltage rating of power devices  $S_a \sim S_d$  is obtained as

$$v_{Sa, stress} = v_{Sb, stress} = v_{Sc, stress} = v_{Sd, stress} = V_{in, max} / 2 = 400V \quad (10)$$

The root-mean-square switch currents  $i_{Sa,rms} \sim i_{Sd,rms}$  are obtained in (11).

$$i_{Sa,rms} = i_{Sd,rms} = i_{La,a,rms} / \sqrt{2} \approx 2.13A \quad (11)$$

MOSFETs SIHG20N50C with 500 V/20 A rating are employed for power devices  $S_a \sim S_d$ . The voltage and average current ratings of diodes  $D_a \sim D_d$  are expressed as

$$v_{Da, stress} = v_{Db, stress} = v_{Dc, stress} = v_{Dd, stress} = 2(V_o + V_f) \approx 49.6V \quad (12)$$

$$i_{Da, av} = i_{Db, av} = i_{Dc, av} = i_{Dd, av} = I_o / 4 = 10A \quad (13)$$

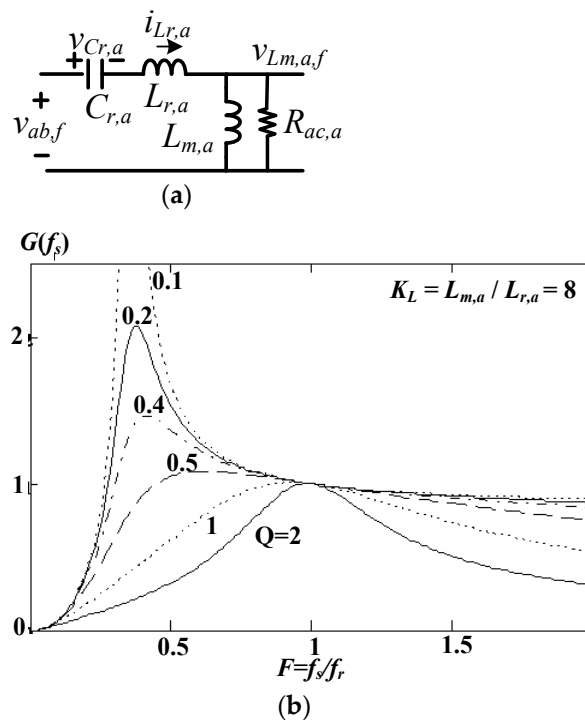


**Figure 6.** The ac resonant tank and voltage gain (a) resonant tank on primary-side of resonant circuit 1 and (b) converter voltage gain.

MBR40100PT with 100 V/40 A ratings are employed for power diodes  $D_a \sim D_d$ . The input capacitances, voltage balance capacitance and output capacitances are  $C_{in,a} = C_{in,b} = 440 \mu\text{F}/450 \text{ V}$ ,  $C_f = 1 \mu\text{F}/630 \text{ V}$  and  $C_o = 4400 \mu\text{F}/100 \text{ V}$ .

## 5. Experimental Results

Experiments are given to confirm the circuit performance. The circuit components of the converter presented are derived in the previous section. Figure 7 demonstrates the test waveforms of  $S_a \sim S_d$  under 100% rated power. It is clear that  $S_a$  ( $S_b$ ) and  $S_c$  ( $S_d$ ) have the same gate signal. Therefore, the square voltage waveforms can be generated on voltages  $v_{ab}$  and  $v_{cd}$ . Due to the converter needing a higher voltage gain at  $V_{in} = 750 \text{ V}$  than  $V_{in} = 800 \text{ V}$ , the switching frequency of  $S_a \sim S_d$  at  $V_{in} = 750 \text{ V}$  input (Figure 7a) is lower than the switching frequency at  $V_{in} = 800 \text{ V}$  input (Figure 7b). Figure 8 provides the test waveforms of  $v_{S_a,gs}$ ,  $v_{S_a,ds}$  and  $i_{S_a}$  at different input voltage and output power conditions. From the experimental results, one can observe that zero voltage switching of  $S_a$  is realized from 5% to 100% load over the whole input voltage range. Since the other switches  $S_c \sim S_d$  have the same circuit characteristics as switch  $S_a$ , it can be concluded that the soft switching operation of  $S_c \sim S_d$  is also accomplished from 5% load to full load. Figure 9 demonstrates the test results of  $v_{C_r,a}$ ,  $v_{C_r,b}$ ,  $i_{L_r,a}$  and  $i_{L_r,b}$  of two half-bridge resonant circuits at 100% rated power. The two currents  $i_{L_r,a}$  and  $i_{L_r,b}$  are well balanced for different input voltage cases. Figure 10 illustrates the experimental waveforms of  $i_{D_a} \sim i_{D_d}$  under 100% rated power. The diode currents are also well balanced between two resonant circuits. Figure 11 gives the test results of  $V_{C_{in,a}}$ ,  $V_{C_{in,b}}$  and  $V_{C_f}$  at 800 V input and 100% rated power. The voltage variation between  $V_{C_{in,a}}$  and  $V_{C_{in,b}}$  is 5 V under full load. The measured circuit efficiencies are 91.4%, 94.8% and 93.7% at 96, 480 and 960 W output power, respectively. The measured switching frequencies are 117 kHz (152 kHz), 110 kHz (135 kHz) and 99 kHz (120 kHz) at 96, 480 and 960 W output load under 750 V (800 V) input operation. Figure 12 provides the test waveforms of the load voltage and load current under load step response. It is clear that the load voltage is stable without serious voltage variation.

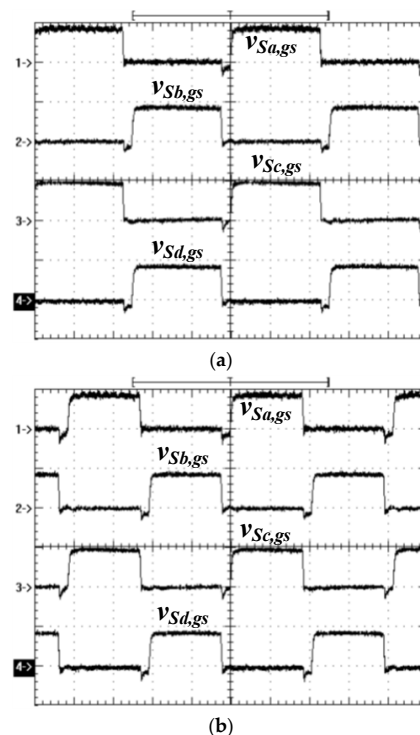


**Figure 7.** Measured waveforms  $v_{S_a,gs} \sim v_{S_d,gs}$  at 100% rated power under (a) 750 V input voltage ( $v_{S_a,gs} \sim v_{S_d,gs}$ : 10 V/div; time: 2  $\mu\text{s}$ ) and (b) 800 V input voltage ( $v_{S_a,gs} \sim v_{S_d,gs}$ : 10 V/div; time: 2  $\mu\text{s}$ ).

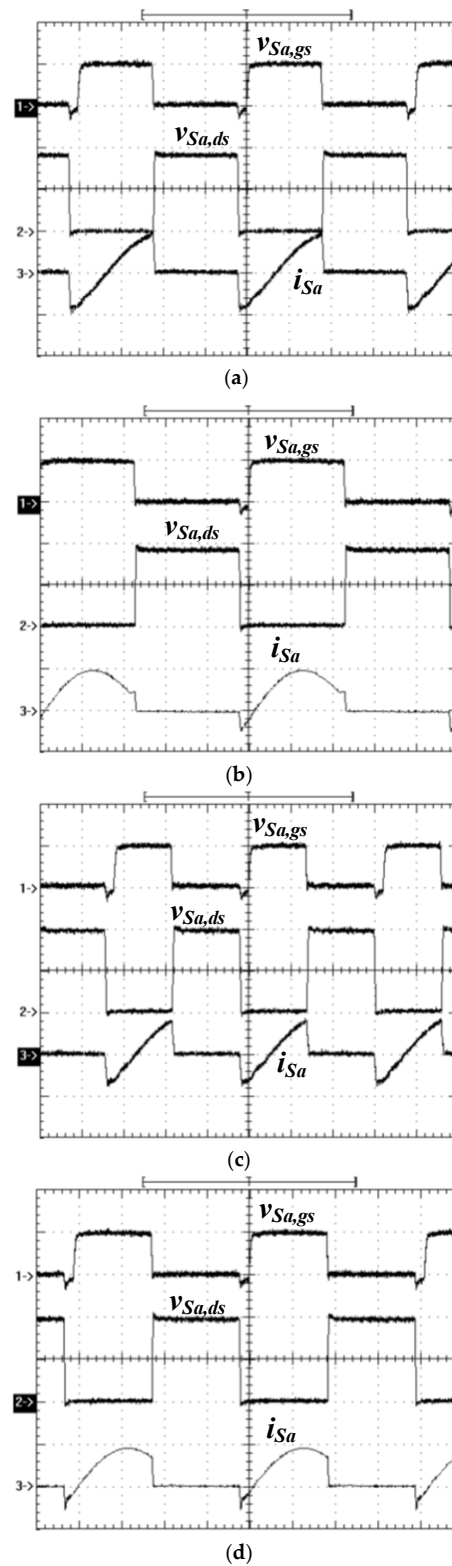


**Figure 8.** Experimental waveforms of  $v_{Sa,gs}$ ,  $v_{Sa,ds}$  and  $i_{Sa}$  under (a) 750 V input and 5% load ( $v_{Sa,gs}$ : 10 V/div;  $v_{Sa,ds}$ : 200 V/div;  $i_{Sa}$ : 2 A/div; time: 2  $\mu$ s), (b) 750 V input and 100% load ( $v_{Sa,gs}$ : 10 V/div;  $v_{Sa,ds}$ : 200 V/div;  $i_{Sa}$ : 5 A/div; time: 2  $\mu$ s), (c) 800 V input and 5% load ( $v_{Sa,gs}$ : 10 V/div;  $v_{Sa,ds}$ : 200 V/div;  $i_{Sa}$ : 2 A/div; time: 2  $\mu$ s) and (d) 800 V input and 100% load ( $v_{Sa,gs}$ : 10 V/div;  $v_{Sa,ds}$ : 200 V/div;  $i_{Sa}$ : 5 A/div; time: 2  $\mu$ s).

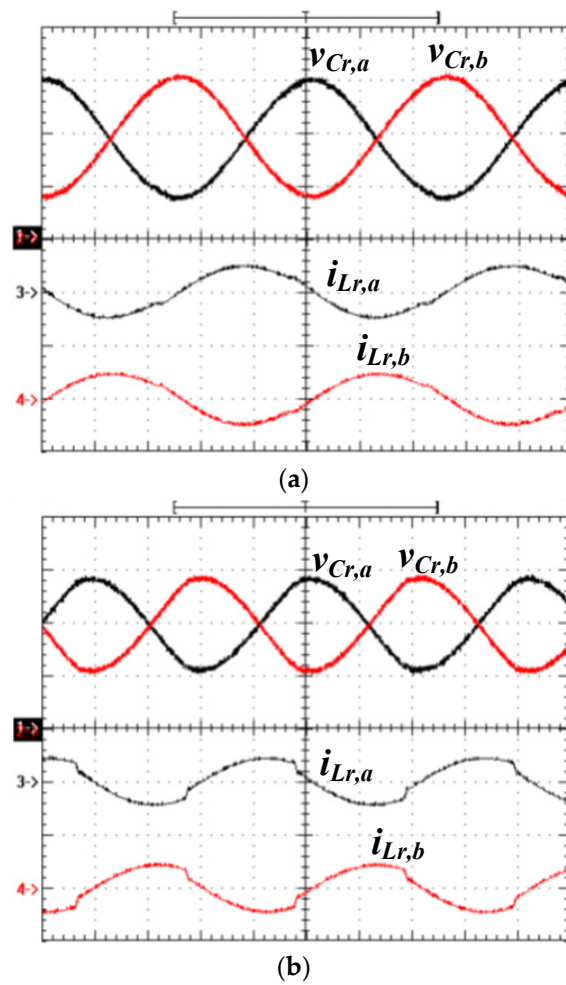


**Figure 9.** Experimental waveforms of  $v_{Cr,a}$ ,  $v_{Cr,b}$ ,  $i_{Lr,a}$  and  $i_{Lr,b}$  at 100% rated power under (a)  $V_{in} = 750$  V ( $v_{Cr,a}$ ,  $v_{Cr,b}$ : 100 V/div;  $i_{Lr,a}$ ,  $i_{Lr,b}$ : 10 A/div; time: 2  $\mu$ s) and (b)  $V_{in} = 800$  V ( $v_{Cr,a}$ ,  $v_{Cr,b}$ : 100 V/div;  $i_{Lr,a}$ ,  $i_{Lr,b}$ : 10 A/div; time: 2  $\mu$ s).

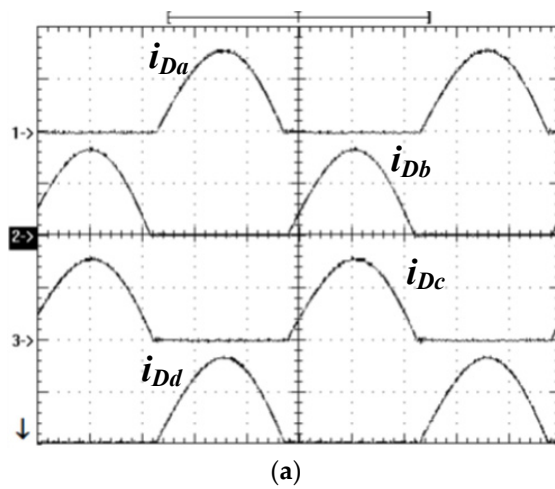


**Figure 10.** Cont.

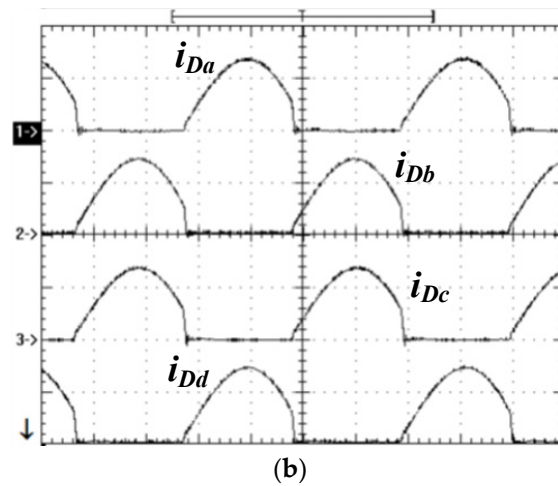


**Figure 10.** Experimental waveforms of  $i_{Da}$ – $i_{Dd}$  at 100% rated power under (a) 750 V input voltage ( $i_{Da}$ – $i_{Dd}$ : 20 A/div; time: 2  $\mu$ s) and (b) 800 V input voltage ( $i_{Da}$ – $i_{Dd}$ : 20 A/div; time: 2  $\mu$ s).

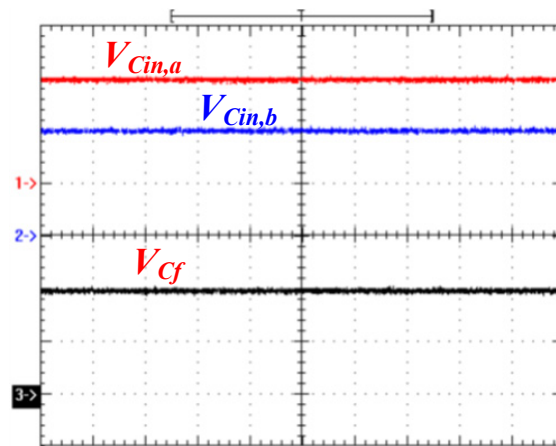


**Figure 11.** Experimental waveforms of  $V_{Cin,a}$ ,  $V_{Cin,b}$  and  $V_{Cf}$  at 800 V input and 100% rated power ( $V_{Cin,a}$ ,  $V_{Cin,b}$ ,  $V_{Cf}$ : 200 V/div; time: 2  $\mu$ s).

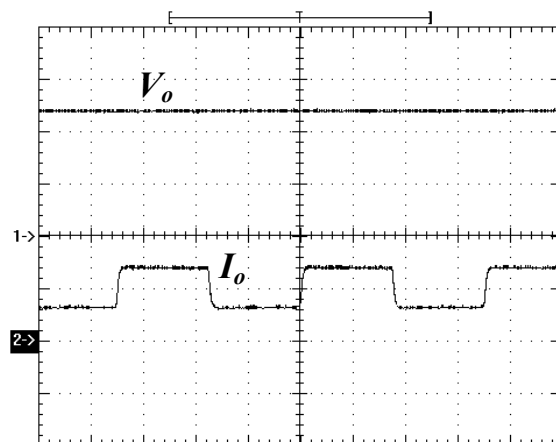


**Figure 12.** Experimental waveforms of  $V_o$  and  $I_o$  under load variation between  $I_o = 12$  and 24 A ( $V_o$ : 10 V/div;  $I_o$ : 20 A/div; time: 200  $\mu$ s).

## 6. Conclusions

A series–parallel connected resonant circuit with the benefits of low current and voltage ratings, balance voltage on active switches, balance current on power components,

and soft switching operation on power devices is proposed, discussed and implemented in this paper. The voltage balance of input split capacitors is achieved by a flying capacitor. The current sharing of two resonant tanks is realized by a magnetic-coupling core. Frequency-control modulation is used to adjust voltage gain of the *LLC* converter. Therefore, the load voltage is well controlled for different input voltage and output current. Since the resonant circuit is worked at the inductive impedance, power semiconductors can be controlled at soft switching operation. The converter presented can be applied in DC light rail vehicles and a DC microgrid bipolar voltage system with high voltage input applications. Finally, experimental tests are given and demonstrate the practicability of the proposed circuit.

**Funding:** This research is supported by the Ministry of Science and Technology (MOST), Taiwan, under grant number MOST 108-2221-E-224-022-MY2.

**Acknowledgments:** The author would like to thank Zong-Xian Xie for his help with measuring the circuit waveforms in the experiment. The author is grateful to the editor and all reviewers for their valuable suggestions to improve this paper.

**Conflicts of Interest:** The author declares no conflict of interest.

## References

1. Song, B.M.; McDowell, R.; Bushnell, A.; Ennis, J. A three-level dc–dc converter with wide-input voltage operation for ship-electric power-distribution systems. *IEEE Trans. Plasma Sci.* **2004**, *32*, 1856–1863. [[CrossRef](#)]
2. Fu, D.X.; Lee, F.C.; Qiu, Y.; Wang, F. A novel high-power-density three-level LCC resonant converter with constant-power-factor-control for charging applications. *IEEE Trans. Power Electron.* **2008**, *23*, 2411–2420. [[CrossRef](#)]
3. Dragicevic, T.; Lu, X.; Vasquez, J.C.; Guerrero, J.M. DC microgrids—Part I: A review of control strategies and stabilization techniques. *IEEE Trans. Power Electron.* **2016**, *31*, 4876–4891. [[CrossRef](#)]
4. Dragicevic, T.; Lu, X.; Vasquez, J.C.; Guerrero, J.M. DC microgrids—Part II: A review of power architectures, applications, and standardization issue. *IEEE Trans. Power Electron.* **2016**, *31*, 3528–3549. [[CrossRef](#)]
5. Chua, T.Z.Y.; Ong, Y.T.; Toh, C.L. Transformerless DC traction power conversion system design for light-rail-transit (LRT). In Proceedings of the IEEE Conference on Energy Conversion (CENCON), Kuala Lumpur, Malaysia, 30–31 October 2017; pp. 38–43.
6. Akagi, H. Classification, terminology, and application of the modular multilevel cascade converter (MMCC). *IEEE Trans. Power Electron.* **2011**, *26*, 3119–3130. [[CrossRef](#)]
7. Lee, J.P.; Min, B.D.; Kim, T.J.; Yoo, D.W.; Yoo, J.Y. Input-Series-Output-Parallel Connected DC/DC Converter for a Photovoltaic PCS with High Efficiency under a Wide Load Range. *J. Power Electron.* **2010**, *10*, 9–13. [[CrossRef](#)]
8. Tao, X.; Li, Y.; Sun, M. A pi-based control scheme for primary cascaded H-bridge rectifier in transformerless traction converters. In Proceedings of the International Conference on Electrical Machines and Systems (ICEMS), Incheon, Korea, 10–13 October 2010; pp. 824–828.
9. Ji, S.; Lu, T.; Zgao, Z.; Yu, H.; Yuan, L. Series-connected HV-IGBTs using active voltage balancing control with status feedback circuit. *IEEE Trans. Power Electron.* **2015**, *30*, 4165–4174. [[CrossRef](#)]
10. Lim, T.C.; Williams, B.W.; Finney, S.J.; Palmer, P.R. Series-connected IGBTs using active voltage control technique. *IEEE Trans. Power Electron.* **2013**, *28*, 4083–4103. [[CrossRef](#)]
11. Chen, W.; Wang, G. Decentralized voltage-sharing control strategy for fully modular input-series-output-series system with improved voltage regulation. *IEEE Trans. Ind. Electron.* **2015**, *62*, 2777–2787. [[CrossRef](#)]
12. Sha, D.; Deng, K.; Liao, X. Duty cycle exchanging control for input-series-output-series connected two PS-FB DC-DC converter. *IEEE Trans. Power Electron.* **2012**, *27*, 1490–1501. [[CrossRef](#)]
13. Lin, B.R.; Cheng, P.J. New ZVS DC-DC converter with series-connected transformers to balance the output currents. *IEEE Trans. Power Electron.* **2014**, *29*, 246–255. [[CrossRef](#)]
14. Ertl, H.; Kolar, J.W.; Zach, F.C. A novel multicell DC-AC converter for applications in renewable energy systems. *IEEE Trans. Ind. Electron.* **2002**, *49*, 1048–1057. [[CrossRef](#)]
15. Perez, M.A.; Bernet, S.; Rodriguez, J.; Kouro, S.; Lizana, R. Circuit topologies, modeling, control schemes, and applications of modular multilevel converters. *IEEE Trans. Power Electron.* **2015**, *30*, 4–17. [[CrossRef](#)]
16. Akagi, H.; Kitada, R. Control and Design of a Modular Multilevel Cascade BTB System Using Bidirectional Isolated DC/DC Converters. *IEEE Trans. Power Electron.* **2011**, *26*, 2457–2464. [[CrossRef](#)]
17. Nami, A.; Liang, J.; Dijkhuizen, F.; Demetriades, G.D. Modular multilevel converters for HVDC applications: Review on converter cells and functionalities. *IEEE Trans. Power Electron.* **2015**, *30*, 18–36. [[CrossRef](#)]
18. Liu, W.; Jin, H.; Yao, W.; Lu, Z. An interleaved PWM method with voltage-balancing ability for half-bridge three-level converter. *IEEE Trans. Power Electron.* **2018**, *33*, 4594–4598. [[CrossRef](#)]

19. Lin, B.R. Interleaved zero-voltage switching three-level converter with less output inductor counts. *IET Proc. Power Electron.* **2017**, *10*, 707–716. [[CrossRef](#)]
20. Song, W.; Ma, J.; Zhou, L.; Feng, X. Deadbeat predictive power control of single-phase three-level neutral-point-clamped converters using space-vector modulation for electric railway traction. *IEEE Trans. Power Electron.* **2016**, *31*, 721–732. [[CrossRef](#)]
21. Lin, B.R. Hybrid dc/dc converter based on dual three-level circuit and half-bridge circuit. *IET Proc. Power Electron.* **2016**, *9*, 817–824. [[CrossRef](#)]
22. Dusmez, S.; Li, X.; Akin, B. A new multi input three-level dc/dc converter. *IEEE Trans. Power Electron.* **2016**, *31*, 1230–1240. [[CrossRef](#)]
23. Haga, H.; Kurokawa, F. A novel modulation method of the full bridge three-level LLC resonant converter for battery charger of electrical vehicles. In Proceedings of the 2015 IEEE Energy Conversion Congress and Exposition, Montreal, QC, Canada, 20–24 September 2015; pp. 5498–5504.
24. Liu, R.; Jones, E.A.; Wang, F.F.; Zhang, Z.; Costinett, D. Capacitor-clamped, three-level Gan-based dc-dc converter with dual voltage outputs for battery charger applications. *IEEE J. Emerg. Sel. Top. Power Electron.* **2016**, *4*, 841–853.
25. Fu, D.; Liu, Y.; Lee, F.C.; Xu, M. A novel driving scheme for synchronous rectifiers in LLC resonant converters. *IEEE Trans. Power Electron.* **2009**, *24*, 1321–1329. [[CrossRef](#)]
26. Gu, Y.; Lu, Z.; Hang, L.; Qian, Z.; Huang, G. Three-level LLC series resonant DC/DC converter. *IEEE Trans. Power Electron.* **2005**, *20*, 781–789. [[CrossRef](#)]
27. Steigerwald, R.L. A comparison of half-bridge resonant converter topologies. *IEEE Trans. Power Electron.* **1988**, *3*, 174–182. [[CrossRef](#)]
28. Liu, C.; Xu, X.; He, D.; Liu, H.; Tian, X.; Guo, Y.; Cai, G.; Ma, C.; Mu, G. Magnetic-coupling current-balancing cells based input-parallel output-parallel LLC resonant converter modules for high-frequency isolation of DC distribution systems. *IEEE Trans. Power Electron.* **2016**, *31*, 6968–6979. [[CrossRef](#)]